Journal of Structural Geology 69 (2014) 32–46

Contents lists available at ScienceDirect

Journal of Structural Geology

journal homepage: www.elsevier.com/locate/jsg

Comparing magnetic and magmatic fabrics to constrain the magma flow record in La Gloria pluton, central Chile

Italo Payacán [a, b, *], Francisco Gutiérrez [a, b], Sarah E. Gelman [c], Olivier Bachmann [c], Miguel Ángel Parada [a]

[a] Departamento de Geología/Centro de Excelencia de Geotermia de los Andes (FONDAP-CEGA), Facultad de Ciencias Físicas y Matemáticas, Universidad de Chile, Santiago 8370450, Chile
[b] Advanced Mining Technology Center, Facultad de Ciencias Físicas y Matemáticas, Universidad de Chile, Santiago 8370451, Chile
[c] Institute of Geochemistry and Petrology, ETH Zurich, Clausiusstrasse 25, 8092 Zurich, Switzerland

ARTICLE INFO

Article history:
Received 22 April 2014
Received in revised form
9 September 2014
Accepted 15 September 2014
Available online 6 October 2014

Keywords:
Magmatic fabric
Magnetic fabric
Convective magma flow
Magma chamber

ABSTRACT

This contribution illustrates a case study of a pluton (La Gloria pluton; LGP) where magnetic and magmatic fabrics are locally decoupled. We compare the magmatic fabric with the available magnetic fabric data to explore their abilities and elucidate the magma flow record of LGP. Results indicate that magnetic (controlled by multi-domain magnetite) and magmatic fabrics are generally consistent throughout LGP. Foliations define an axisymmetric pattern that gradually changes from vertical near lateral margins to less steep in the pluton interior, whereas lineations are subhorizontal following the elongation direction of the pluton. However, samples at the pluton center show marked differences between both fabrics: magnetic fabrics indicate subhorizontal magnetic lineations and foliations, and magmatic fabrics indicate subvertical lineations and foliations.

Both magnetic and magmatic fabrics are interpreted to record strain caused by magma flow during thermal convection and lateral magma propagation at the transition between low and high crystallinity stages. We suggest that fabrics acquisition and consistency were determined by shear conditions (pure/simple shear rates ratio) and the orientation of the magma flow direction with respect to a rigid boundary (critical crystalline region) of the pluton. Magmatic fabric differs at the center of the pluton because pure shear is dominant and ascendant flows are orthogonal to the horizontal rigid boundary. LGP represents a whole-scale partly molten magma reservoir, where both thermal convection and lateral propagation of the magma are recorded simultaneously. This study highlights the importance of characterizing both fabrics to properly interpret magma flow recorded in plutons.

1. Introduction

Petrofabric studies are required to identify textural variations in plutons and can be performed through both field and/or microscopic observations of mineral foliations and lineations, characterizing internal structures, usually to find evidence of magma dynamics (e.g. Hutton, 1988; Paterson et al., 1989, 1998; Bouchez, 1997; Vernon, 2000). Magnetic fabric studies, gained through anisotropy of magnetic susceptibility (AMS) measurements, typically complement this petrological and structural work (e.g. de Saint-Blanquat and Tikoff, 1997; Launeau and Cruden, 1998; de Saint-Blanquat et al., 2001; Trubač et al., 2009; Archanjo et al., 2012). In plutons, AMS has been interpreted as strain directions recorded during different rheological behavior of the magmatic rocks: above-solidus conditions (where the rock is partly melted) and solid-state conditions (with no melt present, where mostly brittle deformation textures are expected; e.g. de Saint-Blanquat and Tikoff, 1997; Archanjo et al., 2008). We distinguish the origin of the recorded strain according to its main driving force: tectonic origin refers to exo-magmatic processes that impact to the pre, syn and post-magmatic system (e.g. a regional fault system acting after the pluton crystallization); whereas a magmatic origin denotes processes in which magma is the driving force (e.g. density gradients of magma). Often, a magmatic origin of AMS fabric is inferred when the magnetic fabric within a pluton differs from regional strain and structures (e.g. McNulty et al., 2000; Petronis et al., 2004;

* Corresponding author. Departamento de Geología/Centro de Excelencia de Geotermia de los Andes (FONDAP-CEGA)/Advanced Mining Technology Center, Facultad de Ciencias Físicas y Matemáticas, Universidad de Chile, Santiago 8370450, Chile. Tel.: +56 9 84398353.
E-mail address: ipayacan@gmail.com (I. Payacán).

http://dx.doi.org/10.1016/j.jsg.2014.09.015
0191-8141/

Stevenson et al., 2007b; Gutiérrez et al., 2013). In the case of magmatic flows arise as a consequence of various processes during the evolution of a magma reservoir, as the building mechanism of plutons, internal magma lobes or sheets movilization, syn-tectonic magma emplacement or convective magmatic flow pattern overprinting the emplacement-related record (e.g. Horsman et al., 2005; Parada et al., 2005; de Saint-Blanquat et al., 2006; Stevenson et al., 2007a; Benn, 2009; Magee et al., 2012; Gutiérrez et al., 2013).

Magnetic fabrics have commonly been interpreted as an indicator of the preferred orientation of crystals and correlated with petrographic fabric (magmatic fabric for plutons) even when the latter is not macroscopically visible (Bouchez, 1997). However, contrary to the case of intrusions where magnetic properties are mainly controlled by ferromagnesian silicates (paramagnetic intrusions; de Saint-Blanquat and Tikoff, 1997; de Luchi et al., 2004), the relationship between magnetic and magmatic fabrics is not necessarily certain when the magnetic properties are controlled by Fe-Ti oxides (e.g. Archanjo et al., 1995; Olivier et al., 1997).

The consistency between the magnetic and magmatic fabrics may be conditioned by "magnetic effects" (Rochette et al., 1992, and references therein). The occurrence of inverse or intermediate magnetic fabric (produced by single-domain and pseudo-single-domain titanomagnetite), the presence of a non-unique magnetic mineralogy, a sub-solidus re-crystallization of magnetic minerals or magnetic interaction of minerals could make more complex the interpretation of magnetic and magmatic fabrics (Grégoire et al., 1995; Lagroix and Borradaile, 2000; Borradaile and Jackson, 2004; Hastie et al., 2011).

Numerical formulation of rotation of elliptical solid-particles embedded in a viscous matrix proposed by Jeffery (1922) has been the basis to simulate the magmatic fabric acquisition in magmas under simple shear strain. Differences between magnetic and magmatic fabrics can be explained in terms of the morphology (aspect ratio) of the crystals controlling each fabric and the nature of the strain affecting the medium (Arbaret et al., 2001; Iezzi and Ventura, 2002; Cañón-Tapia and Chávez-Álvarez, 2004). The different response of crystals under strain may results in the existence of subfabrics in the same mineral group, providing additional complication on the relationship between magnetic and magmatic fabrics (Žák et al., 2005, 2007; Hastie et al., 2011). Hence, the strain patterns recorded in plutons by magnetic fabric need to be complemented with magmatic fabric studies, in order to evaluate the "magnetic anomalies" and the crystal morphology effects during the fabric acquisition.

La Gloria pluton (Central Chile, hereafter LGP) represents a small shallowly emplaced granitic magma body with no sharp internal lithological contacts (Cornejo and Mahood, 1997). Based on comparison between AMS pattern and numerical simulations of the fluid dynamic during the cooling of LGP, Gutiérrez et al. (2013) interpreted the magnetic fabric as a record of strain caused by convective magma flows, but without finding evidence of ascendant magma flow at the center of the pluton. In this work, we pretend to deep into the behavior of crystals during the fabric acquisition, based on a quantitative description and comparison of magnetic and magmatic fabrics, in order to constrain the magma kinematic during the cooling of LGP. We also evaluate the shear strain condition (pure/simple shear rates ratio) necessary to generate the obtained magmatic anisotropy, based on numerical formulations of rotation of rigid particles. This study provides evidences of convective magma flows, including ascendant flows at the center of the pluton as simulated by Gutiérrez et al. (2013). We suggest that the orientation of both fabrics depends on the interplay between the mineral geometry, shear conditions and the relationship of magma flows respect to the rigid borders. This interplay could generate concordance or discordance between magnetic and magmatic fabrics, even, if both fabrics are result of a unique melt-dominated deformation event, as convective flows of the cooling of LGP.

2. La Gloria pluton

2.1. Geological setting

La Gloria pluton (LGP) is a 10 Ma (Cornejo and Mahood, 1997; Deckart et al., 2010) granodiorite/quartz monzonite (with amphibole and biotite), located 35 km east of Santiago, in central Chile (Fig. 1a). LGP is an N30°W elongated magma reservoir with a vertical exposure of 2.5 km, a width of about 4–6 km, and length of 17 km (Fig. 1b). LGP was emplaced during a highly active magmatic period in the central Chilean Andes (both plutonic and volcanic; Vergara et al., 1988), and forms part of an N–S orientated cluster of granitic plutons (Drake et al., 1982, Fig. 1a). LGP intruded Oligocene to Miocene continental volcanic and volcanoclastic rocks (Thiele, 1980), and was emplaced in the core of an anticline at 4–7 km depth (Aguirre, 1960; Cornejo and Mahood, 1997), during a period of intense compressive deformation and crustal thickening (Kay et al., 2005). However, LGP does not exhibit significant field and textural features of post-intrusion tectonic deformation (Cornejo and Mahood, 1997). Plagioclase and amphibole + biotite occur as slightly oriented euhedral to subhedral crystals together with anhedral undeformed and non-aligned interstitial crystals of quartz and K-Feldspar.

2.2. Mineralogical and compositional zonation

Although both vertical and horizontal compositional zones were distinguished (Fig. 1c; Cornejo and Mahood, 1997), mineralogy and composition of La Gloria pluton is mostly homogeneous without well-defined internal contacts, varying only slightly along the main granitic rock. The lower level of the pluton (roughly at 1500–2000 m a.s.l.) is a granodiorite and quartz monzodiorite varying laterally to quartz monzodiorite. Middle levels and borders correspond to quartz monzodiorite, which grades into quartz monzonite towards the upper level, near the roof (up to 4000 m.a.s.l.; Cornejo and Mahood, 1997). Additionally, variations in Hb/(Hb + Bt), Or/(Or + Plag) (Hb: hornblende; Bt: biotite; Or: orthoclase; Plag: plagioclase) have been recognized in LGP, increasing toward the borders and upper level (Cornejo and Mahood, 1997). Accessory minerals include apatite, titanite and Fe-Ti oxides (magnetite-ilmenite; Cornejo and Mahood, 1997). The crystallization sequence inferred from textural relations, and consistent with phase stability, indicates that plagioclase is the earliest mineral, co-crystallizing with amphibole at late stages, followed by biotite, and finally K-feldspar and quartz (Cornejo and Mahood, 1997).

LGP represents a relatively simple fossil magma chamber, that preserves late-magmatic conditions throughout the pluton without internal contacts attributable to multiple intrusive pulses (Cornejo and Mahood, 1997). Sub-solidus re-equilibration was not pervasive (except for Fe-Ti oxides), which suggests that the slight compositional variation identified in LGP reflects late-magmatic conditions (Cornejo and Mahood, 1997). For that reason, LGP represents a suitable case study to constrain the crystal behavior during strain events and determine the magmatic and magnetic fabric acquisition mechanism.

3. Magnetic mineralogy and AMS data

Titanomagnetite is the main magnetic mineral of La Gloria pluton and can be divided into two groups: 1) a major group of individual euhedral to subhedral crystals of 0.1–1 mm, which commonly occur in interstices between silicates crystals (especially

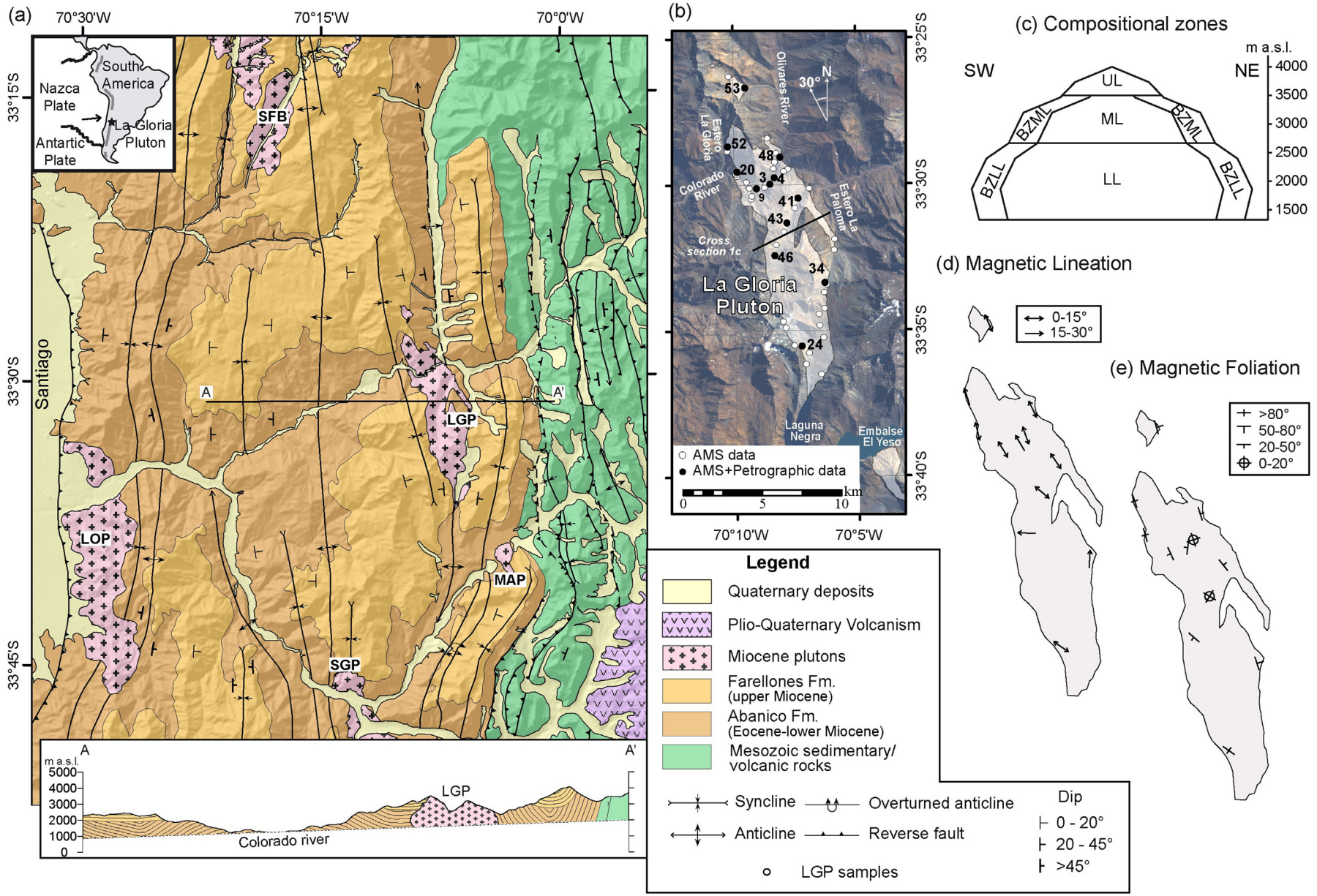

Fig. 1. (a) Geological map of the regional context of La Gloria pluton (LGP) ad cross section showing the relationship with the country rock. Other Miocene plutons are shown: SFB = San Francisco Batholith; LOP = La Obra pluton; MAP = Mesón Alto pluton; SGP = San Gabriel pluton (based on Thiele, 1980; Fock, 2005; Armijo et al., 2010). Map and profiles are obtained from Becker et al. (2009). (b) Field location of samples from La Gloria pluton (black circles represent the sample sites for AMS data used in this study). (c) Schematic cross section of La Gloria pluton (location in Fig. 1b) showing the different zones defined by mineralogical and compositional variations (according to Cornejo and Mahood, 1997). LL = lower level, BZLL = border lower level, ML = middle level, BZML = border middle level, UL = upper level. (d) Distribution of magnetic lineations and (e) distribution of magnetic foliation planes of selected AMS sites for magmatic fabric determination (modified from Gutiérrez et al., 2013).

amphibole and biotite); 2) a secondary crystal group, generally smaller than the first one, occurring as inclusions into silicate minerals. They were re-equilibrated during late-magmatic up to sub-solidus stages, consisting of Ti depleting without evidence of recrystallization (Cornejo and Mahood, 1997). Magnetic experiments (Curie temperature determination and thermal demagnetization experiments) indicate that Ti-poor titanomagnetite multidomain is the main magnetic carrier (see supplementary material 1).

The magnetic fabric of LGP was previously determined by using low-field anisotropy of magnetic susceptibility (AMS; Gutiérrez et al., 2013). The magnetic fabric is mainly oblate with magnetic anisotropy values (up to 1.17) higher at the borders than at the center of the pluton. Magnetic lineations have subhorizontal plunges and NNW trends and are thus aligned with the main elongation direction of the pluton (Fig. 1d). Magnetic foliations are well developed, showing NNW strikes and dips that vary gradually from subvertical at the lateral borders to subhorizontal in the center and at the roof of the pluton (Fig. 1e).

The absence of post-intrusion deformation, the relatively low magnetic anisotropy (<1.15) and the axisymmetric pattern of magnetic foliations are consistent with a magmatic origin, particularly during the late-stage convection when the magma became too crystalline to keep flowing (Gutiérrez et al., 2013).

4. Magmatic fabric determination

In order to compare the magnetic and petrographic fabrics, samples collected at 12 AMS sites (with a similar AMS orientation to the bulk AMS tensor site) were selected as representative of different zones within LGP: the border zones near vertical walls (samples 20, 34, 41, 48, 52 and 53), the center at the lower level (samples 3, 4 and 9) and the upper level near the roof (samples 24, 43 and 46). The used method to determine the magmatic fabric was performed for two mineral groups (plagioclase and amphibole + biotite), each one exhibiting different modal proportions (40–60 vol.% and 10–15 vol.%, respectively). Amphibole and biotite crystals were considered as a unique mineral group because both show similar preferred orientation.

4.1. 2-D and 3-D preferred mineral orientation tensor

Characterization of the magmatic fabric was obtained according to the following steps: (1) the preferred crystal orientations are determined for three orthogonal thin sections per sample; and (2) the petrographic data are combined using an algebraic algorithm to ultimately produce a 3-D magmatic fabric tensor.

2-D petrographic data were obtained for each sample from three thin sections (mineral planes) with orientations perpendicular to the AMS tensor axes ($Pl_{max}\perp K_{max}$; $Pl_{int}\perp K_{int}$ and $Pl_{min}\perp K_{min}$; where Pl is a mineral plane, and K is an AMS tensor axis; Fig. 2a). Length, width and orientation of individual crystals were obtained from thin sections by image analysis using the 2-D analysis tool of JMicroVision software (Roduit, 2008, Fig. 2b). Orientations of each mineral group with respect to the AMS axes were determined for each mineral plane by using a bidirectional Bingham distribution (Stereonet software; Cardozo and Allmendinger, 2013), that is graphically represented by a rose diagram (Fig. 2b). Similar to existing methods of preferred shape orientation (Launeau and Robin, 1996, 2005), 2-D tensor (represented by ellipses) were defined by the average orientation of each mineral group, representing the preferred orientation of crystals (algebraic details are given in supplementary material 2). Tensor axis magnitudes were weighted by crystal lengths, defining the 2-D magmatic anisotropy as the ratio between the major and minor ellipse axes, which depends on the proximity of the crystal population to the mean orientation.

Using the three orthogonal 2-D tensors (ellipses), we found a 3-D tensor for each mineral group based on the method of Shimamoto and Ikeda (1976) and Robin (2002) (algebraic details of the method are presented in supplementary material 2). The 3-D tensor is represented by an ellipsoid with axes $M_{max} \geq M_{int} \geq M_{min}$, where M_{max} corresponds to the preferred crystal length orientation. In order to characterize the magmatic fabric and compare it with the

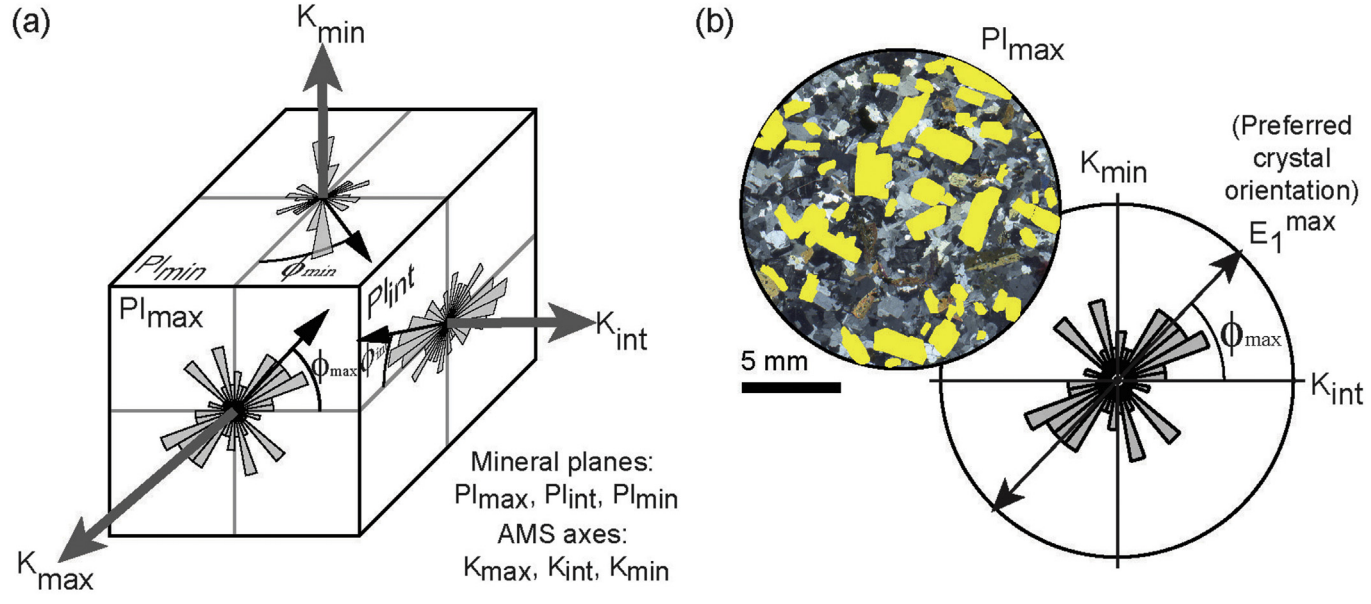

Fig. 2. (a) Thin section planes perpendicular to each magnetic anisotropy axis ($Pl_{max}\perp K_{max}$; $Pl_{int}\perp K_{int}$; $Pl_{min}\perp K_{min}$; where Pl are the mineral planes and K are the magnetic anisotropy axes). Rose diagrams represent the preferred orientation of crystal population characterized by angles ϕ_{max}, ϕ_{int} and ϕ_{min}. (b) Photomicrograph (Pl_{max} as example) showing measured plagioclase crystals. Crystal orientations are plotted in a rose diagram. (E_1^{max}: preferred orientation of crystals; ϕ_{max}: angle respect to the respective AMS axis, according to the mineral plane).

magnetic data, 3-D magmatic anisotropy parameters were defined using the same definition of magnetic anisotropy parameters (Jelinek, 1981): magmatic anisotropy ($P = M_{max}/M_{min}$), magmatic foliation ($F = M_{int}/M_{min}$) and magmatic lineation ($L = M_{max}/M_{int}$). The orientation of the magmatic fabric tensor is characterized by the magmatic lineation, given by the orientation of M_{max}, and the plane of magmatic foliation, normal to the minor axis M_{min}.

4.2. Pure and simple shear condition evaluation

Existing numerical formulations that characterizes the rotation of solid particles embedded in a viscous matrix allow to simulated the fabric evolution under shear strain (Jeffery, 1922; Ghosh and Ramberg, 1976). Nevertheless, the strain magnitude and direction cannot be estimated and compared between different zones of a pluton as La Gloria pluton, because the shear plane is not recognizable in the samples and solutions are not unique (a strain ellipse may be generated by combinations of simple and pure strain in different directions). However, by using the formulation of Ghosh and Ramberg (1976), we simulated the 2-D magmatic anisotropy under different ratios of the relative pure and simple shear rates values and compared the simulated anisotropy with the measured one from mineral plane. This effectively estimates the maximum value of the ratio:

$$S_r = \dot{\varepsilon}/\dot{\gamma} \quad (1)$$

necessary to obtain the measured magmatic anisotropy in LGP samples, where $\dot{\varepsilon}$ and $\dot{\gamma}$ are relative values of pure and simple shear rates, respectively. When $S_r = 0$, it represents a strain with simple shear without pure shear.

The formulation was applied separately on the three mineral planes to identify differences of magmatic anisotropy and shear conditions between their directions, characterizing the three ortogonal components of the strain that affected each sample. We considered as input the crystal sizes and aspect ratios measured on thin sections for plagioclase (roughly 100 crystals per mineral plane) and amphibole + biotite crystals (roughly 50 crystals per mineral plane), all of them initially randomly oriented. Some numerical and experimental studies of particle orientation show that the anisotropy and preferred orientation tend to stabilize around a mean value as shear strain is applied (Ildefonse et al., 1997; Cañón-Tapia and Chávez-Álvarez, 2004). In order to obtain a statistically representative result of the anisotropy value of stabilization, we considered that the viscous matrix containing the measured crystals was subjected to long simple shear interval (γ from 0 to 250 in steps of 0.5). Additionally, we considered pure/simple shear ratios (S_r) of 0, 0.1, 0.25, 0.5, 0.75 and 1. Then, the simulated anisotropy was compared with the measured magmatic anisotropy in samples, determining the maximum relative shear strain rates ratio necessary to yield the magmatic anisotropy in each analyzed section.

5. Results: the magmatic fabric of La Gloria pluton

5.1. 2-D petrographic data based on crystal length

2-D magmatic fabric tensors were obtained for each mineral plane in samples of LGP, considering roughly 100 crystals for plagioclase (with mean aspect ratio of 2 ± 0.5) and 50 crystals for amphibole + biotite (with mean aspect ratio of 2 ± 0.8) per section. Results indicate that the mean orientation between both mineral groups is generally consistent (Fig. 3). Additionally, the preferred crystal orientations of each mineral group are considered as statistically representative of the crystal population. Evidences of subfabrics are not found for plagioclase and amphibole + biotite, where the preferred orientations of crystals are consistent grouping crystals with different size or aspect ratio (see supplementary material 3).

Mean magmatic anisotropy values are similar for both mineral groups, but the mean value depends on the mineral plane and the field location within LGP. Samples near the vertical walls have similar 2-D magmatic anisotropy values for the three mineral planes (roughly 1.3; Fig. 4). In contrast, samples located at the center of the pluton have higher 2-D magmatic anisotropy and present differences between the mineral planes (particularly for amphibole + biotite), giving ~ 1.3, 1.4 and 1.5 for the planes Pl_{max}, Pl_{min} and Pl_{int}, respectively (Fig. 4).

The highest 2-D magmatic anisotropy values and the best fit between mean crystal length orientations and AMS axes are obtained for the plane perpendicular to the intermediate AMS axis (Pl_{int}), where the maximum (K_{max}) and minimum (K_{min}) AMS axes are contained and highest magnetic anisotropy is obtained (Fig. 4). This is observed because the preferred mineral orientations are relatively closer to the maximum AMS axis in Pl_{int} than other planes, differing in 2°±27° (α95) for plagioclase and 9°±24° (α95) for amphibole + biotite. This indicates that the 2-D preferred mineral orientations are consistent with AMS data, although some differences emerge locally. For example: 2-D magmatic anisotropy is higher in Pl_{min} than in Pl_{max} (Fig. 4), contrary to the magnetic fabric. Additionally, the mean magmatic anisotropy differences between the mineral planes are about 0.1–0.2, indicating similar magnitudes of magmatic lineation and foliation; whereas magnetic fabric is mainly oblate (anisotropy values are much higher in Pl_{int} and Pl_{max} than in Pl_{min}).

5.2. 3-D magmatic fabric

The 3-D magmatic fabric is characterized for selected samples through orientation tensors fitted to an ellipsoid for each mineral group (table in supplementary material 4). Magmatic anisotropy (P) ranges from 1.2 to 2.5 for plagioclase, and from 1.11 to 2.7 for amphibole + biotite, whereas magmatic lineation values are generally higher than foliation values (L between 1.0 and 2.2 and F between 1.0 and 1.6; Fig. 5a). The shape parameter values (T) indicate that the magmatic fabric tensor has mainly a prolate shape for plagioclase and amphibole + biotite. Sample 9 yields the highest magmatic anisotropy value and is located at center of the lower level of the pluton, where the macroscopic magmatic fabric is most obvious.

In order to compare the anisotropy parameters obtained for plagioclase and amphibole + biotite, for each sample, we define the slope (S) of the straight line that correlates the magmatic parameter values of amphibole + biotite with respect to those of plagioclase in Fig. 5a. $S > 1$ indicates relatively higher anisotropy values for amphibole + biotite, while $S < 1$ indicates higher anisotropy values for plagioclase. S values are higher than 0.7 for samples located at the center of the pluton, while samples near the borders have S values lower than 0.7 (Fig. 5b). This indicates that the magmatic anisotropy parameter values (specifically P) are relatively higher for plagioclase than amphibole + biotite in samples located near the walls, compared to samples at the center of the pluton.

Orientations of the magmatic tensors change consistently for plagioclase and amphibole + biotite, and depend on the field location of the samples with respect to vertical walls. Samples located near the borders of LGP present subhorizontal mean lineations (considering both mineral groups) with an NNW trend and a plunge of 22° ± 17° (Fisher confidence angle α95; Fig. 5c); whereas foliation planes are mainly subvertical and parallel to the walls (Fig. 5d). However, the magmatic foliation plane orientations are poorly defined probably because the elongated crystal shapes of

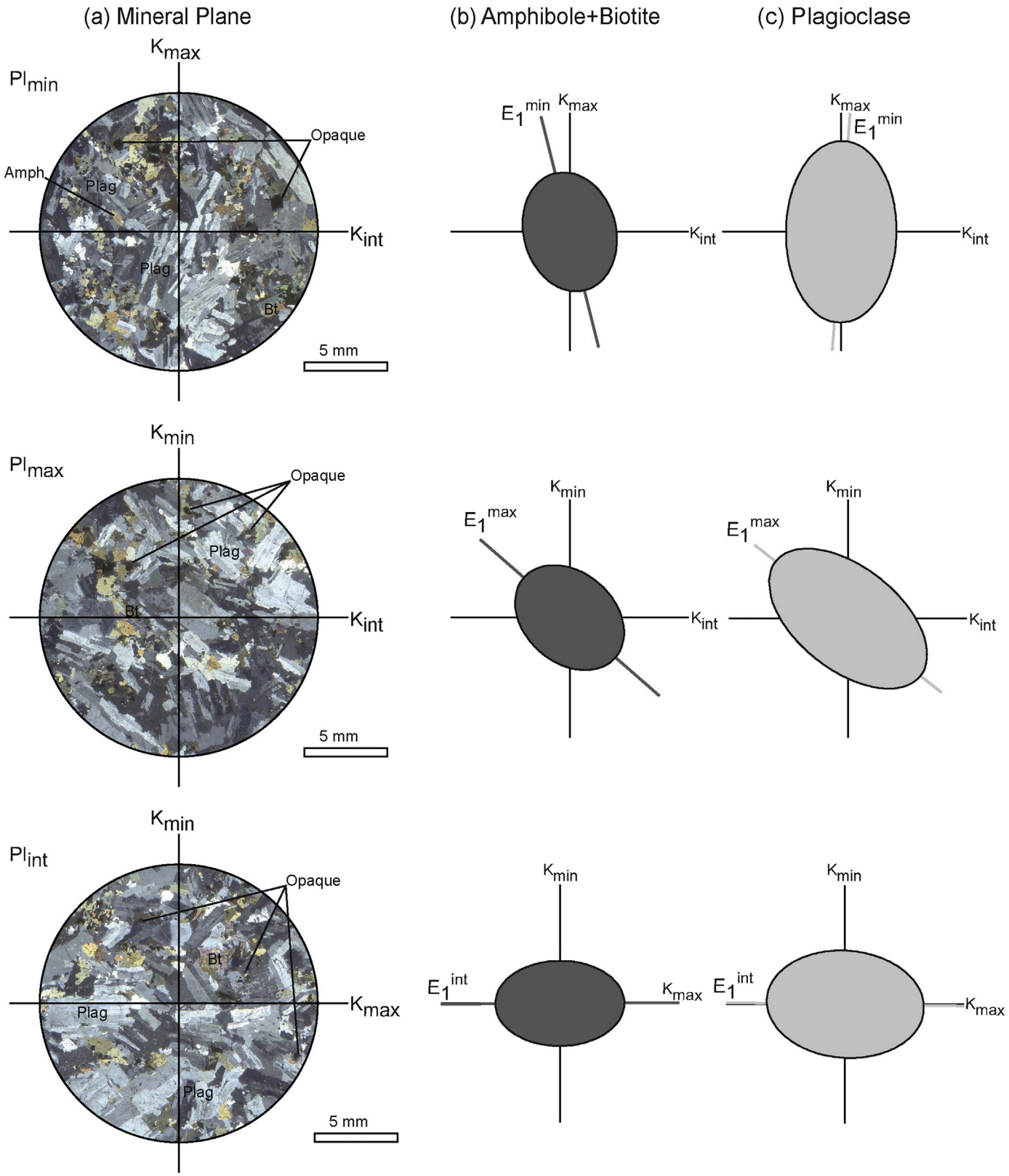

Fig. 3. (a) Photomicrographs (cross-Nichols) oriented with respect to the AMS tensor axes (K_{max}, K_{int} and K_{min}) for sample 34 (orientation of mineral planes in Fig. 2a). Some minerals are labeled (Plag: plagioclase; Bt: biotite; Amph: amphibole; Opaque: opaque minerals, mostly titanomagnetite). (b) 2-D tensors of crystal length orientations (ellipses) obtained for amphibole + biotite in each mineral plane. (c) 2-D tensors of crystal length orientations (ellipses) obtained for plagioclase in each mineral plane. AMS axes and main crystal orientations (eigenvalues: E_1) are shown for each 2-D tensor.

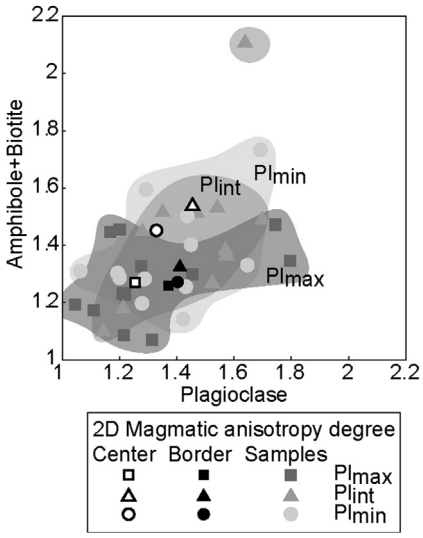

Fig. 4. 2-D anisotropy values given by the preferred orientation of crystal lengths for plagioclase and amphibole + biotite. Mean values for each mineral plane are shown grouping the samples located near the vertical walls (black symbols) and near the center and the roof of the pluton (white symbols).

plagioclase and amphibole. Orientations of magmatic fabric in border samples match well with magnetic fabric orientation, which yields NNW subhorizontal lineations and vertical foliation planes, parallel to the margins of LGP (Fig. 5e).

Although some samples at the center of the pluton exhibit magmatic fabric tensors similar to those at the borders (e.g. samples 3 and 4), other samples (samples 9, 24 and 46) yield steeper magmatic lineations than magnetic lineations (Fig. 6). These samples have lineations with NNW trends and plunge of 80 ± 21° (Fig. 5c) and magmatic foliation planes mainly subvertical (Fig. 5d). This orientation is found in the lower zone (sample 9) and the upper central zone (samples 24 and 46) of the pluton, as well as along its long axis.

5.3. Crystal length preferred orientation and shear conditions

Results indicate that 2-D magmatic anisotropy tends to oscillate around a mean value as shear strain is applied on crystal populations, producing a range of anisotropy values (Fig. 7a; see Video 1 in supplementary material), which is consistent with previous studies (Ildefonse et al., 1997; Cañón-Tapia and Chávez-Álvarez, 2004; Arbaret et al., 2013). For each sample, we considered the lower limit of the 2σ interval of the simulated 2-D magmatic anisotropy as the least statistically possible anisotropy that can be generated under each shear condition (relative pure and simple shear ratio S_r; Eq. (1)). The simulated 2-D magmatic anisotropy increases when a relatively higher pure shear rate is applied to crystals (higher S_r; Fig. 7b and c). Thus, each mineral group yields a maximum S_r necessary to generate the measured 2-D anisotropy in each plane. Because plagioclase and amphibole + biotite coexisted when magmatic fabric was acquired, we considered the maximum S_r value that could affect the crystals (S_r^*) in each mineral plane as the minimum value between S_r obtained for both mineral groups. It is worth noting that for a given sample, the plane with the lowest S_r^* represents the direction where simple shear strain mainly controls the preferred crystal orientation. Thus, the axis normal to the plane with the lowest S_r^* represents the maximum stretching direction during the magmatic fabric acquisition.

Most of the obtained 2-D and 3-D mineral anisotropies are reached with S_r lower than 0.5 (low pure shear conditions). High anisotropy samples (9, 53, 34, 24 and 46) correspond to samples where the highest S_r values (>0.5) are obtained for both mineral groups. Samples that have vertical crystal elongations (i.e. vertical M_{max} at 9, 24 and 46) have lower S_r^* values in subhorizontal planes than at subvertical planes, indicating vertical maximum stretching zones. This indicates that these samples had a maximum stretching in a subvertical direction, which is consistent with the maximum 3-D crystal elongations of both mineral groups. These samples are located at the pluton interior and/or below the pluton roof. On the contrary, samples near the vertical walls of LGP tend to present much lower S_r values, indicating that the magmatic fabric was recorded mostly under simple shear strain conditions in these zones, at the expense of pure shear strain.

6. Discussion: the nature of the magmatic and magnetic fabric

6.1. Comparison between magnetic and magmatic fabrics

The consistency between the magnetic and magmatic fabrics and the lack of evidence of pervasive brittle and sub-solidus deformation (see section 2.1), imply that magmatic fabric defined by plagioclase and amphibole + biotite is a record of strain during a partly molten stage of LGP (above-solidus conditions). In addition, these minerals occur with anhedral undeformed and non-aligned interstitial crystals of quartz and K-Feldspar, suggesting that they crystallized at the final stage of magma solidification and unaffected by deformation near the solidus. The strain recorded by both fabrics may be caused by: 1) a magmatic origin (e.g. magma convection); or 2) a tectonic origin (e.g. a fault system). Because the magnetic and magmatic fabrics are consistent with the borders of the pluton and differ with the regional structural patterns, we support the first option, interpreting both the magnetic and magmatic fabrics as a record of the strain produced by magma flows. The strain was recorded in the rheological locking zone during the transition between the low and high crystallinity stages (i.e., in the critical crystallinity region with ~55–60 vol% crystals; Marsh, 1996), reflecting the last period of magma convection. This is consistent with the modal content of the analyzed minerals.

Although magnetic and magmatic fabrics are generally coincident, the consistency between both fabrics does not universally occur in the pluton interior. For example, samples 9 and 46 at the center of LGP has a magmatic foliation that is subvertical and a magnetic foliation that is subhorizontal, whereas the magmatic lineation is subvertical and the magnetic lineation is subhorizontal (Fig. 6). We discard inverse magnetic fabrics that could explain the disparity between both fabrics (Rochette et al., 1992, and references therein), because termomagnetic experiments suggest that multidomain Ti-poor titanomagnetite is the magnetic carrier and there is no evidence of magnetite recrystallization during sub-solidus stages. This suggests that the magma flow that would control the two fabrics may have different characteristics in the center and near the margins of the pluton, and understanding these characteristics may provide new insights into the magnetic and magmatic fabrics acquisition mechanism.

In the case of LGP, differences between magnetic and magmatic fabrics could represent a primary feature given by the preferred mineral orientation of plagioclase and amphibole + biotite, and a secondary feature given by titanomagnetite alignment. This can be possible by the generation of an earlier network by plagioclase and amphibole + biotite with a primary fabric, whereas titanomagnetite in the interstices acquired a later subfabric (e.g. Žák et al., 2008; Hastie et al., 2011; Žák and Kabele, 2012; Picard et al., 2013).

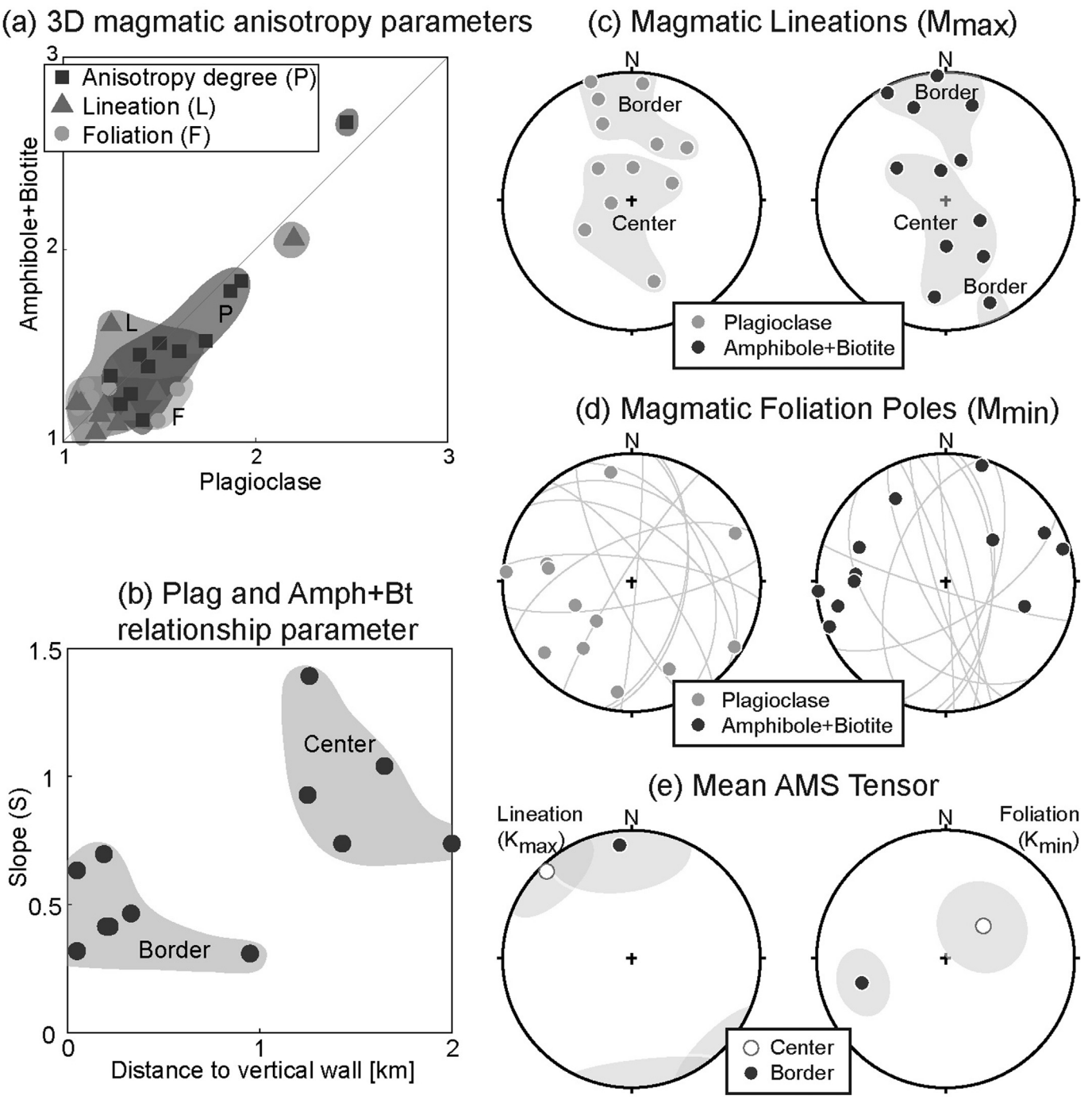

Fig. 5. (a) Magmatic anisotropy parameters of La Gloria pluton for plagioclase and amphibole + biotite. (b) Parameter of comparison (S) values, defined for each sample as the slope of the straight line that fits the anisotropy parameter values in the plot (a), with respect to the distance to the nearest vertical wall. (c), (d) and (e) are stereographic projection (lower hemisphere equal area) of: (c) magmatic lineations (M_{max}), grouped according to location within the pluton (center and border); (d) poles of the magmatic foliation planes (M_{min}); (e) mean magnetic lineations and poles of magnetic foliation planes at the center and the borders of the pluton for samples analyzed in this work (from Gutiérrez et al., 2013). Gray areas represent the α95 confidence angle calculated using the Fisherian statistics.

However, in that case, plagioclase and amphibole + biotite crystals would show evidence of reorientation with plastic and/or brittle deformation textures produced by the secondary strain event that yielded the magnetic fabric. We suggest that magnetic and magmatic fabrics were caused by a unique strain event, where titanomagnetite and silicates were oriented as independent solid-particles, because titanomagnetite crystals are mainly present in interstices associated with the edges of silicate minerals (Fig. 3a).

Differences between magnetic and magmatic fabrics in LGP could be explained by considering the morphologic characteristics of the mineral group that define each fabric. Plagioclase, amphibole and biotite, that define the magmatic fabric, have higher aspect ratio than titanomagnetite crystals, which control the magnetic fabric. We evaluated the effect of the aspect ratio of the particles following the formulation of Ghosh and Ramberg (1976), confirming the results of existing models of free-rotation of solid particles

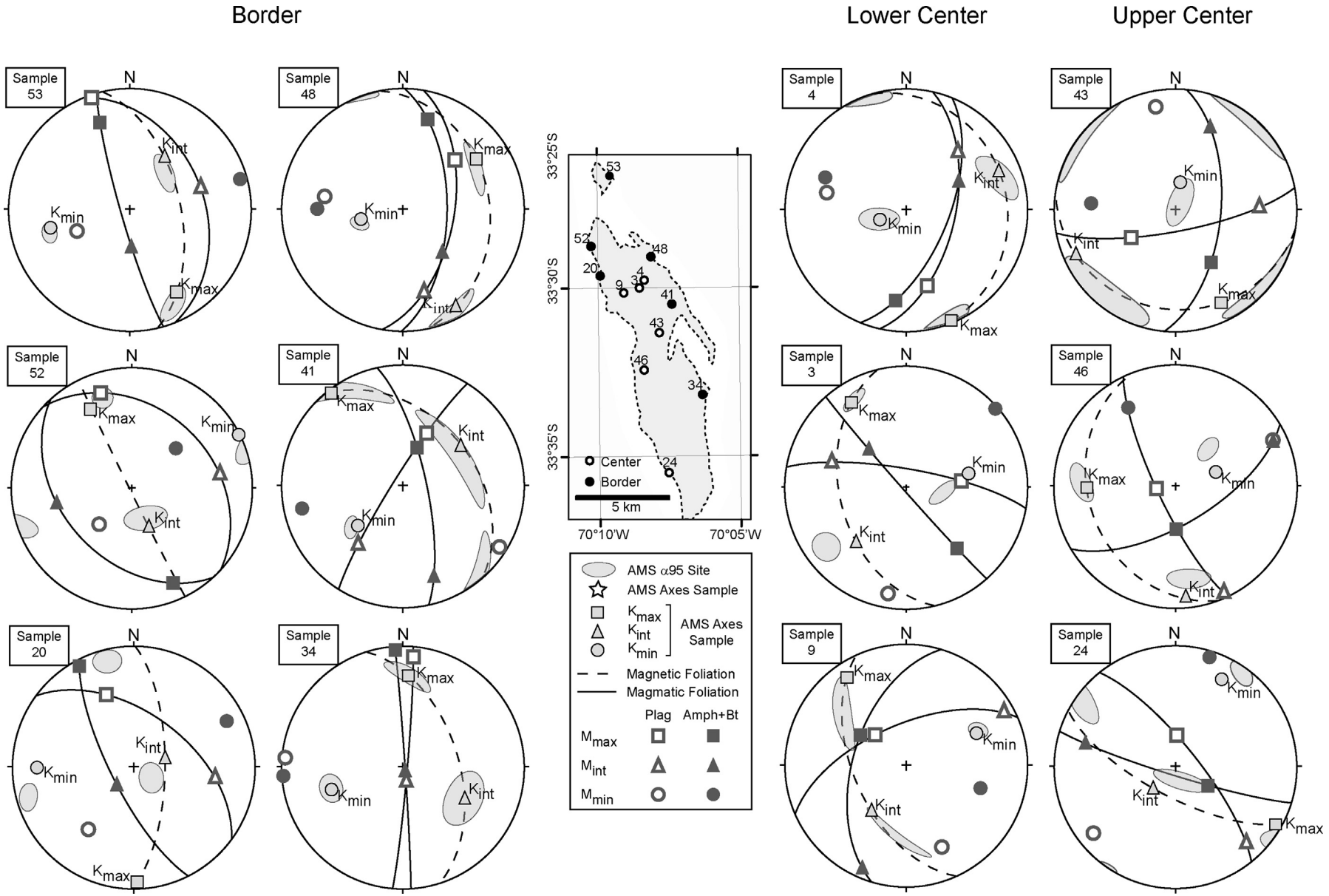

Fig. 6. Stereographic projection (lower hemisphere equal area) of the magmatic anisotropy axes, grouped in samples located at the center (lower and upper levels) and the borders of LGP. The magnetic fabric axes of each sample and the associated site error (α95, gray area) are plotted for comparison (taken from Gutiérrez et al., 2013).

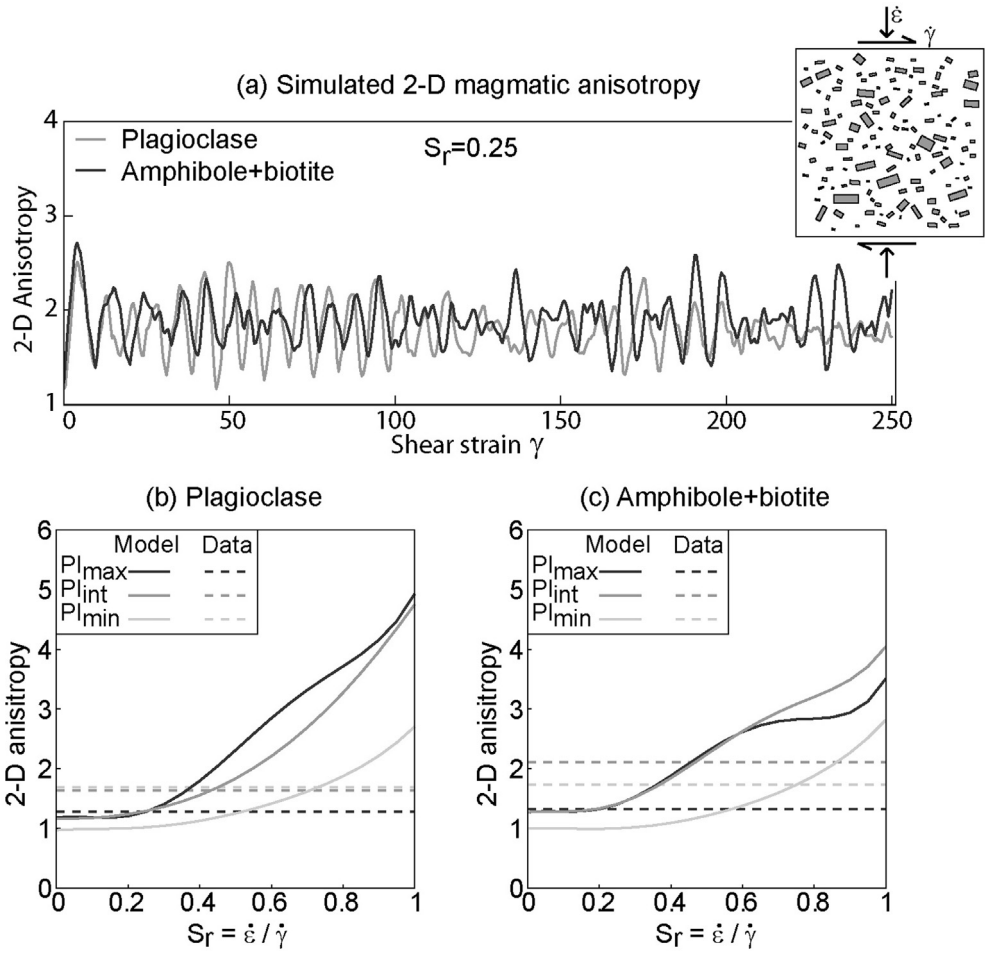

Fig. 7. (a) Example of simulated 2-D magmatic anisotropies for plagioclase and amphibole + biotite in a mineral plane. Box on the corner represents a scheme of crystal population and simple ($\dot{\gamma}$) and pure ($\dot{\varepsilon}$) shear applied in simulations. (b) and (c) show an example of the lower 2σ interval limit of the simulated 2-D magmatic anisotropy values under different S_r values for both plagioclase and amphibole + biotite, respectively. 2-D magmatic anisotropy increases when higher pure shear rates than simple shear rates is applied (higher S_r values).

embedded in a viscous matrix under shear conditions, that indicate that particles with higher aspect ratio tend to orient more easily than particles with lower aspect ratio (Ghosh and Ramberg, 1976; Launeau and Cruden, 1998; Arbaret et al., 2001; Cañón-Tapia and Chávez-Álvarez, 2004) (see supplementary material 5 for details). When shear strain is applied on theoretical crystal groups with aspect ratios of 1.01 (orientable isometric crystals), 2.00 and 3.50, preferred orientations close to the shear plane are obtained for the three groups (0°, 6° and 11°, respectively). However, the highest dispersions of crystal orientations are obtained for isometric crystals, obtaining a roughly isotropic fabric (see supplementary material 5). This suggests that only high aspect ratio minerals are able to be oriented under simple and pure shear conditions. Because of the mean measured aspect ratios for plagioclase and amphibole + biotite is 2, these minerals would be expected to re-orient under such shear strain yielding a defined preferred crystal orientation of crystal population. On the contrary, the preferred orientation of titanomagnetite crystals (isometric) is unaffected by shear, yielding a disperse orientation of crystal population.

The dependence of the preferential orientation of crystals as a function of their morphology suggests that magnetic fabric given by AMS measurements is controlled by magnetic interaction of titanomagnetite crystal alignments (Hargraves et al., 1991; Grégoire et al., 1995), but not by orientation of individual crystals. Titanomagnetite crystal alignments can be controlled by silicate crystal borders and/or by magma shear strain along a rigid surface acting as a boundary layer during the pluton cooling (the critical crystallinity region; Marsh, 1996). We opt for the second option because most titanomagnetite crystals are not aligned at the border of silicate crystals. In addition, if titanomagnetite crystals were aligned around silicate crystal borders, magnetic and magmatic fabrics would be consistent throughout the pluton. Although ferromagnetic inclusions inside ferromagnesian silicates can also complicate the magnetic and magmatic fabrics interpretation (Lagroix and Borradaile, 2000), the main titanomagnetite population occurs as individual crystals at interstices between silicate minerals. Although titanomagnetites in LGP were re-equilibrated during late-magmatic stages up to sub-solid conditions, this does not disturb the crystals distribution that control the magnetic fabric of LGP and re-equilibration of Fe-Ti oxides took place when magma was too crystalline to keep flowing.

Another difference between the pluton interior and border zones is the nature of the strain that affected the magma during its cooling: pure or simple shear (S_r values, Eq. (1)). Coincidentally, samples at the center of the pluton with the highest differences between magmatic and magnetic fabrics (e.g. samples 9, 24, 46) also yield the highest magmatic anisotropy values and present the highest pure shear rate (with respect to simple shear rate) necessary to obtain the crystal orientation. This condition of relatively high pure shear strain favored the vertical orientation of crystals with high aspect

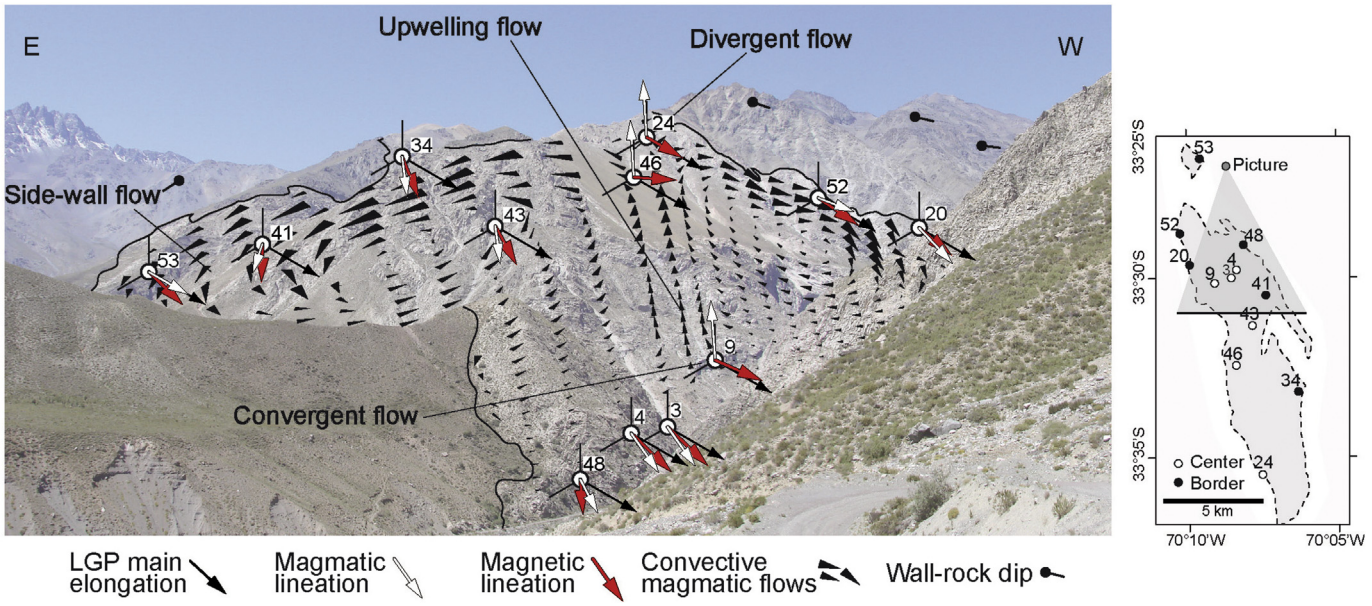

Fig. 8. Section of LGP showing the convective magma flow pattern and the magmatic and magnetic fabric. Magma flow pattern is given by convection (black cones proportional to the flow velocity of the numerical simulation of convection pattern of Gutiérrez et al. (2013) and lateral magma migration in the main orientation of LGP. Red arrows represent the 3-D magmatic lineations and blue arrows represent the magnetic lineations. Samples are projected to represent its relative position inside the pluton. (For interpretation of the references to colour in this figure legend, the reader is referred to the web version of this article.)

ratio (plagioclase and amphibole + biotite) and probably controlled the difference between magmatic and magnetic fabric. The nature of the forces that gave place to both the magnetic and magmatic fabrics of LGP is discussed in the following section.

6.2. Magnetic and magmatic fabrics as a record of magmatic flow

Differences in the magmatic fabric along LGP provide new insight into the nature of the magma flow during its cooling. Results indicate that magmatic fabric is mainly controlled by plagioclase at the borders of the pluton (yielding higher anisotropy values than amphibole + biotite; Fig. 5b), and by plagioclase and amphibole + biotite at the center of the pluton (similar anisotropy values for both mineral groups; Fig. 5b). This difference is dependent on the location inside the pluton, and can potentially be related to cooling rates expected in LGP. Shear strain acted for a shorter interval time near the borders because faster cooling rates are expected, compared to the center of the pluton. This causes that the relatively earlier phases (plagioclase for LGP) becomes oriented, but not later phases as amphibole + biotite, which crystallized during the last crystallization period of plagioclase. On the contrary, both mineral groups determine the magmatic fabric at the center because the slower cooling rates and longer interval time of shear strain allow for amphibole + biotite to acquire a preferred crystal orientation similar to plagioclase. This suggests that the simple shear rate (higher at the border than at the center of the pluton; Gutiérrez et al., 2013) is not the only variable to orientate crystals, but also the magnitude of pure shear, the amount of shear strain, the crystallization sequence and the cooling rate also play important roles.

Samples near the borders of LGP (and some near the center) exhibit magmatic and magnetic subhorizontal lineations following the main elongation of the pluton and subvertical foliations parallel to vertical walls of the pluton (e.g. samples 4, 34 and 52). This pattern indicates that both types of fabrics record strain caused by magmatic flows parallel to the pluton contact in a subhorizontal direction following the main elongation of LGP. Because of LGP was emplaced along the core of an anticline with strike hinge axis similar to the main elongation of the pluton (Figs. 1a and 8), it is likely that the magma was emplaced horizontally in an NNW-SSE direction, through the core of the anticline and postdating the tectonic deformation. This is relationship observed in several cases by field studies and analogous models of magma emplacement along thrust and folded belts (e.g. Kalakay et al., 2001; Musumeci et al., 2005; Montanari et al., 2010; Ferré et al., 2012).

In the case of LGP, Mahood and Cornejo (1992) proposed that upward flows transported high differentiated magma, which could result in vertical magnetic and magmatic fabrics. However, this transport occurred as leucogranitic layers with well-defined borders that could not affect the surrounding fabrics pervasively. On the contrary, fluid dynamics numerical simulations of LGP reproduce the convection pattern given by descending flows at the borders and an ascending plume at the center of the reservoir, without any replenishing or feeder magma zones (Fig. 8; Gutiérrez et al., 2013). This proposed model is also supported by the relative compositional and mineralogical homogeneity of the pluton: although some compositional zones are identified in LGP (Cornejo and Mahood, 1997), the pluton has a narrow compositional range without sharp internal contacts. The strain caused by the magma convection was recorded by the magnetic foliation (Gutiérrez et al., 2013). However, the ascending magma flow at the center of LGP did not appear to be recorded by magnetic fabric, which instead yields subhorizontal magnetic foliations at the inner zones of the pluton (Fig. 5e). Despite this, the magmatic fabric of some samples near the center of the pluton (samples 9, 24 and 46) provide evidence for such vertical flow pattern, because: (1) vertical magmatic lineations are obtained at inner zones of LGP; (2) sample 9, located at the lower part of LGP center, yields the highest magmatic anisotropy values, consistent with convergent flows (Iezzi and Ventura, 2002), which are predicted at the base of a convective system (Paterson et al., 1998; and references therein); and (3) higher S_r^* values and vertical maximum stretching directions obtained for these samples are also consistent with convergent flows at the center of the pluton. We conclude that the magmatic and magnetic fabrics are determined by the nature of the shear strain instead by the simple

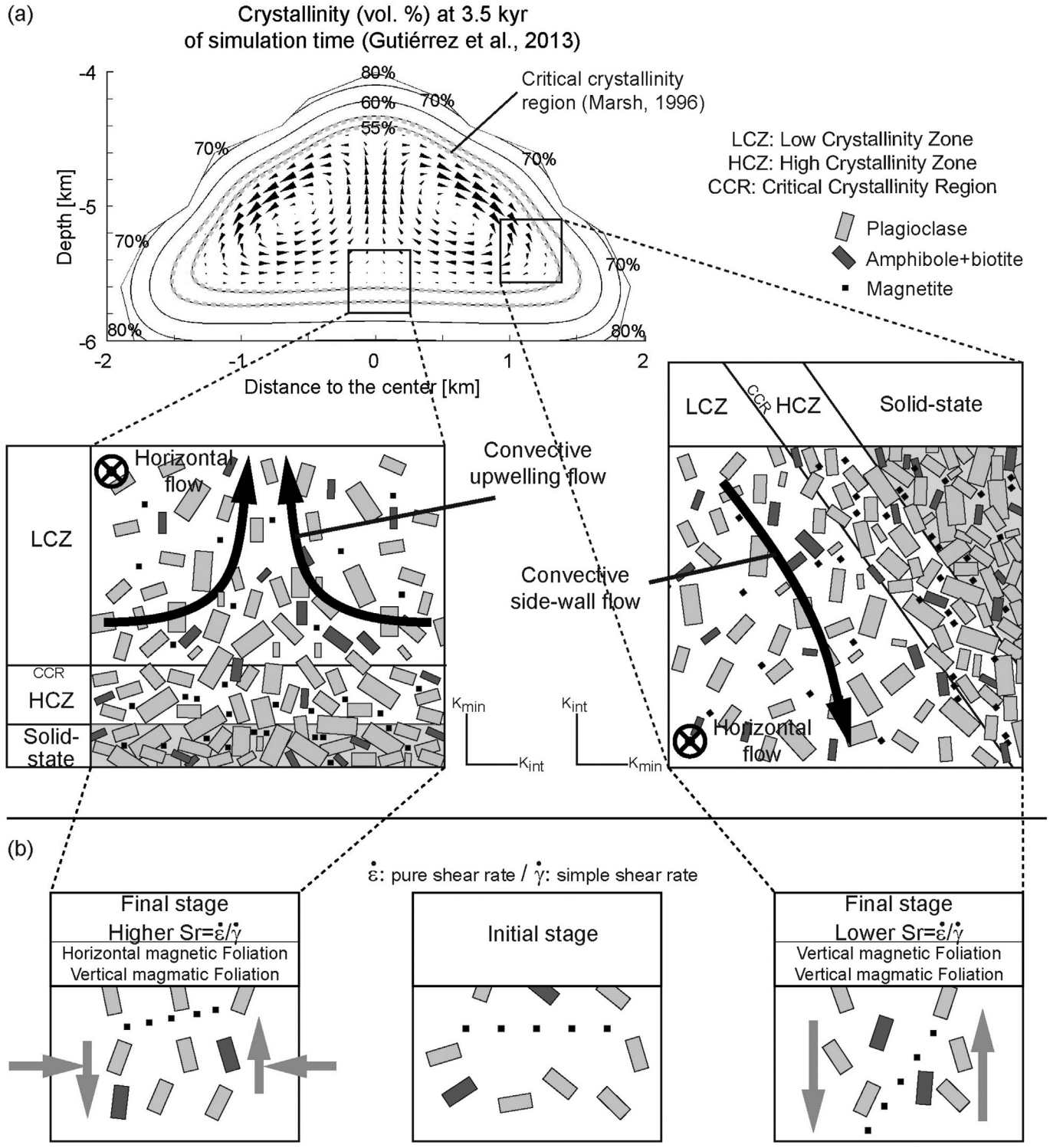

Fig. 9. Scheme that represents the magnetic and magmatic fabric acquisition mechanism at the lower level of the center and the border of LGP. (a) Rheological domains are distinguished during the cooling of LGP, respect to the simulated simple convection pattern (Gutiérrez et al., 2013): (1) mobile magma, with crystallinity lower than ~55 vol.% (LCZ); (2) a high crystallinity zone (HCZ) with crystallinity higher than ~55vol.%; and (3) a solid-state domain, where magma was totally crystallized. Both magnetic and magmatic fabrics are recorded in the transition between the LCZ and HCZ (CCR: critical crystallinity region; Marsh, 1996). Sketches (squares) present a comparison between the magmatic flow directions and crystals dispositions at border and the lower center of LGP. (b) Sketches of the magnetic and magmatic fabrics acquisition under different shear strain conditions, depending on the location inside LGP. Near the vertical walls and mainly simple shear strain (with lower pure shear strain) magnetite crystals tend to align parallel to the main orientation of the elongated crystals. At the center of the pluton, convergent flows yield that elongated crystals tend to orientate vertically and titanomagnetite crystals tend to be closer conserving the foliation parallel to the horizontal CCR, produced by the cooling advancing front.

shear rate. This interpretation of magmatic and magnetic fabrics differences suggest that pure shear has a strong impact in orienting high aspect ratio minerals (i.e. the magmatic fabric) but a minimum effect for the titanomagnetite alignment (i.e. magnetic fabric). The pure shear effect explains the highest magmatic anisotropy at the center of the pluton.

We suggest that the vertical magmatic and magnetic foliations along the borders of LGP recorded magma flow with relatively low pure shear strain, parallel to the expected critical crystallinity zone that acts as a boundary layer (Fig. 9a). These flows allowed titanomagnetite crystals to be aligned following the orientation of elongated silicate crystals, because magma flow is parallel to the rigid surface. On the contrary, at the center of LGP we interpret that titanomagnetite crystals are horizontally aligned, parallel to the critical crystallinity region at the base of the pluton; whereas elongated crystals (plagioclase and amphibole + biotite) tend to orient vertically according to the ascending magmatic flow (Fig. 9a). This may be controlled by the interplay of two conditions: 1) the expected rigid boundary layer at the center of the pluton has a horizontal disposition, perpendicular to the ascendant magma flow, allowing titanomagnetite crystals acquiring a subhorizontal disposition consistent with the cooling front; and 2) the higher magmatic anisotropy at the center than the borders of the pluton and the vertical magmatic lineations suggest that the strain was caused by a convergent flow (Iezzi and Ventura, 2002), where the pure shear strain was dominant at the expense of simple shear (samples with the highest S_r values). As simulations of particles rotation indicate, elongated crystals tend to be strongly orientated perpendicular to pure shear strain directions (Ghosh and Ramberg, 1976; Iezzi and Ventura, 2002; this work). However, in the case of titanomagnetite crystal previously aligned horizontally with the cooling front, the pure shear strain is unable to orientate them vertically (Fig. 9b). Indeed a geometric analysis of the orientation of crystal alignments under different applied pure shear strain indicates that horizontal alignments tend to conserve their orientation (rotation is lower than 20°) when shortening is lower than 50% (see supplementary material 6).

We propose that magnetic fabric registered the shear strain along the inward advancing critical crystallinity region, representing the boundary layer (horizontal at the pluton center); whereas magmatic fabric records the shear strain related to the flow directions (vertical at the pluton interior). We suggest that magmatic and magnetic fabrics differ in plutons where pure shear is predominant, particularly at the center of the pluton, where simulated convection indicates convergent and divergent magma flows perpendicular to the rigid cooling front. Because magma convection and the associated pure shear at the center of the magma reservoir depends on the cooling rate, differences between magmatic and magnetic fabrics are expected to be higher in small (<10 km width) and shallow (<10 km depth) plutons, where higher cooling rates are expected.

In La Gloria pluton, the magnetic and magmatic fabrics record the strain caused by both magma convection (downward wall-side flows and an upward central flow) and lateral propagation of the reservoir (following the pluton elongation direction). This suggests that the pluton construction had a first stage, where LGP was a whole-scale partially molten magma reservoir with crystallinity lower than 55–60 %vol., representing entirely an individual active magma chamber of ~200 km^3. The high compositional and mineralogical homogeneity and the lack of sharp internal contacts suggest that the reservoir was highly homogenized by magma flows and stirring (Bachmann and Bergantz, 2008; Huber et al., 2009), resulting in a simply cooling system. Once the magma reservoir construction proceeds, both convection and lateral propagation were registered simultaneously. Several studies have proposed that plutons are assembled by amalgamation of small incremental magma pulses as sills and/or dikes (Coleman et al., 2004; Glazner et al., 2004; Walker et al., 2007). This process was not recorded in LGP, probably because it was early in the magma reservoir evolution and the record was erased during the homogenization stage. However, pulses may have been injected in a horizontal direction, following the lineation trend, as large-scale magma flows across the width, controlling the lateral magma propagation and without disrupting the convection record.

7. Conclusions

Magmatic fabric was determined in numerous samples of the LGP using 2-D textural data of individual crystals for two independent mineral families: plagioclase and amphibole + biotite. Based on these textural data, 3-D tensors (ellipsoids) and magmatic anisotropy parameters were calculated and compared with the magnetic fabric of LGP. This work illustrates a case study of a pluton where magnetic and magmatic fabrics are locally decoupled.

Both fabrics in LGP are commonly consistent presenting foliation plane variations from parallel at the walls to less steep at the pluton interior. Lineations are commonly subhorizontal following the main elongation of the pluton. Some samples at the center of the pluton, having the highest magmatic anisotropy and the higher relative pure/simple shear rates compared with samples near the borders, exhibit marked differences of both fabric orientations: in these samples the magnetic fabric recorded subhorizontal lineations and foliation planes, whereas the magmatic fabric recorded subvertical lineations and foliation planes. We interpret subhorizontal lineations as consequence of lateral migration of the magma in the main pluton elongation direction (N–NW), and foliations and vertical magmatic lineations as consequence of simple thermal convection, both recorded simultaneously.

Magnetic and magmatic fabrics were recorded during above-solidus conditions, recording the last strain caused by magmatic flows. They were registered mostly at the rheological transition from fluid to solid behavior along critical crystallinity region (~55–60 vol% crystals) growing from the edge, which acts as a rigid boundary layer, toward the pluton interior. We suggest that magnetic fabric recorded the shear strain produced by magma flows along the rigid boundary layer (recording the inward advancing critical crystallinity region), whereas magmatic fabric indicates the magma flow direction. Magmatic and magnetic fabrics are decoupled at the center of the pluton, because lateral pure shear strain, caused by convergent magma flows, tends to orient elongated crystals vertically with high anisotropy compared to other zones; whereas magnetite crystal alignments remain horizontal, parallel to the rigid border of the cooling front. These results, together with previous numerical simulations, support that La Gloria pluton represents a whole-scale partially molten individual magma chamber of ~200 km^3, where both convection and lateral propagation were registered simultaneously.

We emphasize the importance of characterizing both the magnetic and magmatic fabrics in plutons in order to identify properly magma flow processes during pluton solidification.

Acknowledgments

This research has been developed by the FONDECYT N°11100241 and PBCT-PDA07 projects granted by CONICYT (Chilean National Commission for Science and Technology). Payacán is supported by CONICYT master grant N°22130729. Gutiérrez and Bachmann were supported by U.S. National Science Foundation (NSF) grant EAR-080982 during the completion of this paper. We also thank to D. Carrizo for their helpful comments on the regional geological

background. Comments and suggestions provided by the reviewers S. Paterson, C Archanjo and K. Benn are deeply appreciated.

Appendix A. Supplementary data

Supplementary data related to this article can be found at http://dx.doi.org/10.1016/j.jsg.2014.09.015.

References

Aguirre, L., 1960. Geología de los Andes de Chile central (provincia de Aconcagua), Santiago. Inst. Investig. Geol. Bol. 9, 70.

Arbaret, L., Launeau, P., Diot, H., Sizaret, S., 2013. Magnetic and shape fabrics of magnetite in simple shear flows. J. Volcanol. Geotherm. Res. 249, 25–38.

Arbaret, L., Mancktelow, N.S., Burg, J.-P., 2001. Effect of shape and orientation on rigid particle rotation and matrix deformation in simple shear flow. J. Struct. Geol. 23, 113–125.

Archanjo, C., Campanha, G., Salazar, C., Launeau, P., 2012. Using AMS combined with mineral shape preferred orientation analysis to understand the emplacement fabrics of the Apiaí gabbro-norite (Ribeira Belt, SE Brazil). Int. J. Earth Sci. 101, 731–745.

Archanjo, C.J., Hollanda, M.H.B.M., Rodrigues, S.W.O., Neves, B.B.B., Armstrong, R., 2008. Fabrics of pre- and syntectonic granite plutons and chronology of shear zones in the Eastern Borborema Province, NE Brazil. J. Struct. Geol. 30, 310–326.

Archanjo, C.J., Launeau, P., Bouchez, J.L., 1995. Magnetic fabric vs. magnetite and biotite shape fabrics of the magnetite-bearing granite pluton of Gameleiras (Northeast Brazil). Phys. Earth Planet. Inter. 89, 63–75.

Armijo, R., Rauld, R., Thiele, R., Vargas, G., Campos, J., Lacassin, R., Kausel, E., 2010. The West Andean Thrust, the San Ramón Fault, and the seismic hazard for Santiago, Chile. Tectonics 29.

Bachmann, O., Bergantz, G.W., 2008. Rhyolites and their source mushes across tectonic settings. J. Petrol. 49, 2277–2285.

Becker, J., Sandwell, D., Smith, W., Braud, J., Binder, B., Depner, J., Fabre, D., Factor, J., Ingalls, S., Kim, S., 2009. Global bathymetry and elevation data at 30 arc seconds resolution: SRTM30_PLUS. Mar. Geod. 32, 355–371.

Benn, K., 2009. Anisotropy of magnetic susceptibility fabrics in syntectonic plutons as tectonic strain markers: the example of the Canso pluton, Meguma Terrane, Nova Scotia. Earth Environ. Sci. Trans. R. Soc. Edinb. 100, 147–158.

Borradaile, G.J., Jackson, M., 2004. Anisotropy of Magnetic Susceptibility (AMS): Magnetic Petrofabrics of Deformed Rocks. Geological Society, London, Special Publications 238, pp. 299–360.

Bouchez, J., 1997. Granite is never isotropic: an introduction to AMS studies of granitic rocks. Granite: Segreg. Melt Emplace. Fabr. 8, 95–112.

Cañón-Tapia, E., Chávez-Álvarez, M., 2004. Rotation of uniaxial ellipsoidal particles during simple shear revisited: the influence of elongation ratio, initial distribution of a multiparticle system and amount of shear in the acquisition of a stable orientation. J. Struct. Geol. 26, 2073–2087.

Cardozo, N., Allmendinger, R.W., 2013. Spherical projections with OSXStereonet. Comput. Geosci. 51, 193–205.

Coleman, D.S., Gray, W., Glazner, A.F., 2004. Rethinking the emplacement and evolution of zoned plutons: geochronologic evidence for incremental assembly of the Tuolumne Intrusive Suite, California. Geology 32, 433–436.

Cornejo, P.C., Mahood, G.A., 1997. Seeing past the effects of re-equilibration to reconstruct magmatic gradients in plutons: La Gloria Pluton, central Chilean Andes. Contrib. Mineral. Petrol. 127, 159–175.

de Luchi, M.L., Rapalini, A., Siegesmund, S., Steenken, A., 2004. Application of Magnetic Fabrics to the Emplacement and Tectonic History of Devonian Granitoids in Central Argentina. Geological Society, London, Special Publications 238, pp. 447–474.

de Saint-Blanquat, M., Habert, G., Horsman, E., Morgan, S.S., Tikoff, B., Launeau, P., Gleizes, G., 2006. Mechanisms and duration of non-tectonically assisted magma emplacement in the upper crust: the Black Mesa pluton, Henry Mountains, Utah. Tectonophysics 428, 1–31.

de Saint-Blanquat, M., Law, R.D., Bouchez, J.-L., Morgan, S.S., 2001. Internal structure and emplacement of the Papoose Flat pluton: an integrated structural, petrographic, and magnetic susceptibility study. Geol. Soc. Am. Bull. 113, 976–995.

de Saint-Blanquat, M., Tikoff, B., 1997. Development of magmatic to solid-state fabrics during syntectonic emplacement of the Mono Creek granite, Sierra Nevada batholith. In: Granite: from Segregation of Melt to Emplacement Fabrics. Kluwer Academic Publishers, pp. 231–252.

Deckart, K., Godoy, E., Bertens, A., Jerez, D., Saeed, A., 2010. Barren Miocene granitoids in the Central Andean metallogenic belt, Chile: geochemistry and NdHf and UPb isotope systematics. Andean Geol. 37, 1–31.

Drake, R., Vergara, M., Munizaga, F., Vicente, J.C., 1982. Geochronology of Mesozoic-Cenozoic magmatism in central Chile, Lat. 31°-36°S. Earth-Sci. Rev. 18, 353–363.

Ferré, E.C., Galland, O., Montanari, D., Kalakay, T.J., 2012. Granite magma migration and emplacement along thrusts. Int. J. Earth Sci. 101, 1673–1688.

Fock, A., 2005. Cronología y tectónica de la exhumación en el Neógeno de los Andes de Chile central entre los 33° y los 34°S. Departamento de Geología. Universidad de Chile, p. 179. Unpublished.

Ghosh, S., Ramberg, H., 1976. Reorientation of inclusions by combination of pure shear and simple shear. Tectonophysics 34, 1–70.

Glazner, A.F., Bartley, J.M., Coleman, D.S., Gray, W., Taylor, R.Z., 2004. Are plutons assembled over millions of years by amalgamation from small magma chambers? GSA Today 14, 4–12.

Grégoire, V., de Saint Blanquat, M., Nédélec, A., Bouchez, J.L., 1995. Shape anisotropy versus magnetic interactions of magnetite grains: experiments and application to AMS in granitic rocks. Geophys. Res. Lett. 22, 2765–2768.

Gutiérrez, F., Payacán, I., Gelman, S.E., Bachmann, O., Parada, M.A., 2013. Late-stage magma flow in a shallow felsic reservoir: merging the anisotropy of magnetic susceptibility record with numerical simulations in La Gloria Pluton, central Chile. J. Geophys. Res. Solid Earth 118, 1984–1998.

Hargraves, R., Johnson, D., Chan, C., 1991. Distribution anisotropy: the cause of AMS in igneous rocks? Geophys. Res. Lett. 18, 2193–2196.

Hastie, W.W., Aubourg, C., Watkeys, M.K., 2011. When an 'inverse'fabric is not inverse: an integrated AMS-SPO study in MORB-like dykes. Terra Nova 23, 49–55.

Horsman, E., Tikoff, B., Morgan, S., 2005. Emplacement-related fabric and multiple sheets in the Maiden Creek sill, Henry Mountains, Utah, USA. J. Struct. Geol. 27, 1426–1444.

Huber, C., Bachmann, O., Manga, M., 2009. Homogenization processes in silicic magma chambers by stirring and mushification (latent heat buffering). Earth Planet. Sci. Lett. 283, 38–47.

Hutton, D.H., 1988. Granite emplacement mechanisms and tectonic controls: inferences from deformation studies. Trans. R. Soc. Edinb. Earth Sci. 79, 245–255.

Iezzi, G., Ventura, G., 2002. Crystal fabric evolution in lava flows: results from numerical simulations. Earth Planet. Sci. Lett. 200, 33–46.

Ildefonse, B., Arbaret, L., Diot, H., 1997. Rigid particles in simple shear flow: is their preferred orientation periodic or steady-state? Granite: from Segregation of Melt to Emplacement Fabrics. Springer, pp. 177–185.

Jeffery, G.B., 1922. The motion of ellipsoidal particles immersed in a viscous fluid. Proc. R. Soc. Lond. Ser. A, Contain. Pap. a Math. Phys. Character 102, 161–179.

Jelinek, V., 1981. Characterization of the magnetic fabric of rocks. Tectonophysics 79, T63–T67.

Kalakay, T.J., John, B.E., Lageson, D.R., 2001. Fault-controlled pluton emplacement in the Sevier fold-and-thrust belt of southwest Montana, USA. J. Struct. Geol. 23, 1151–1165.

Kay, S.M., Godoy, E., Kurtz, A., 2005. Episodic arc migration, crustal thickening, subduction erosion, and magmatism in the south-central Andes. Geol. Soc. Am. Bull. 117, 67–88.

Lagroix, F., Borradaile, G.J., 2000. Magnetic fabric interpretation complicated by inclusions in mafic silicates. Tectonophysics 325, 207–225.

Launeau, P., Cruden, A.R., 1998. Magmatic fabric acquisition mechanisms in a syenite: results of a combined anisotropy of magnetic susceptibility and image analysis study. J. Geophys. Res. 103, 5067–5089.

Launeau, P., Robin, P.-Y., 1996. Fabric analysis using the intercept method. Tectonophysics 267, 91–119.

Launeau, P., Robin, P.-Y.F., 2005. Determination of fabric and strain ellipsoids from measured sectional ellipses: implementation and applications. J. Struct. Geol. 27, 2223–2233.

Magee, C., Stevenson, C.T.E., O'Driscoll, B., Petronis, M.S., 2012. Local and regional controls on the lateral emplacement of the Ben Hiant Dolerite intrusion, Ardnamurchan (NW Scotland). J. Struct. Geol. 39, 66–82.

Mahood, G.A., Cornejo, P.C., 1992. Evidence for ascent of differentiated liquids in silicic magma chamber found in a granitic pluton. Trans. R. Soc. Edinb. 83, 63–69.

Marsh, B.D., 1996. Solidification fronts and magmatic evolution. Mineral. Mag. 60, 5–40.

McNulty, B.A., Tobish, O.T., Cruden, A.R., Gilder, S., 2000. Multi-stage emplacement of the Mount Givens pluton, central Sierra Nevada batholith, California. Geol. Soc. Am. Bull. 112, 119–135.

Montanari, D., Corti, G., Sani, F., Del Ventisette, C., Bonini, M., Moratti, G., 2010. Experimental investigation on granite emplacement during shortening. Tectonophysics 484, 147–155.

Musumeci, G., Mazzarini, F., Corti, G., Barsella, M., Montanari, D., 2005. Magma emplacement in a thrust ramp anticline: the Gavorrano Granite (northern Apennines, Italy). Tectonics 24.

Olivier, P., de Saint Blanquat, M., Gleizes, G., Leblanc, D., 1997. Homogeneity of granite fabrics at the metre and dekametre scales. Granite: from Segregation of Melt to Emplacement Fabrics. Springer, pp. 113–127.

Parada, M.A., Roperch, P., Guiresse, C., RamArez, E., 2005. Magnetic fabrics and compositional evidence for the construction of the Caleu pluton by multiple injections, Coastal Range of central Chile. Tectonophysics 399, 399–420.

Paterson, S.R., Fowler Jr., T.K., Schmidt, K.L., Yoshinobu, A.S., Yuan, E.S., Miller, R.B., 1998. Interpreting magmatic fabric patterns in plutons. Lithos 44, 53–82.

Paterson, S.R., Vernon, R.H., Tobisch, O.T., 1989. A review of criteria for the identification of magmatic and tectonic foliations in granitoids. J. Struct. Geol. 11, 349–363.

Petronis, M., Hacker, D., Holm, D., Geissman, J., Harlan, S., 2004. Magmatic Flow Paths and Palaeomagnetism of the Miocene Stoddard Mountain Laccolith, Iron Axis region, Southwestern Utah, USA. Geological Society, London, Special Publications 238, pp. 251–283.

Picard, D., Arbaret, L., Pichavant, M., Champallier, R., Launeau, P., 2013. The rheological transition in plagioclase-bearing magmas. J. Geophys. Res. Solid Earth 118 (4), 1363–1377.

Robin, P.-Y.F., 2002. Determination of fabric and strain ellipsoids from measured sectional ellipses—theory. J. Struct. Geol. 24, 531–544.
Rochette, P., Jackson, M., Aubourg, C., 1992. Rock magnetism and the interpretation of anisotropy of magnetic susceptibility. Rev. Geophys. 30, 209–226.
Roduit, N., 2008. JMicroVision: Image Analysis Toolbox for Measuring and Quantifying Components of High-definition Images. Version 1.2. 7.
Shimamoto, T., Ikeda, Y., 1976. A simple algebraic method for strain estimation from deformed ellipsoidal objects. 1. Basic theory. Tectonophysics 36, 315–337.
Stevenson, C.T., Owens, W.H., Hutton, D.H., 2007a. Flow lobes in granite: the determination of magma flow direction in the Trawenagh Bay Granite, northwestern Ireland, using anisotropy of magnetic susceptibility. Geol. Soc. Am. Bull. 119, 1368–1386.
Stevenson, C.T.E., Owens, W.H., Hutton, D.H.W., Hood, D.N., Meighan, I.G., 2007b. Laccolithic, as opposed to cauldron subsidence, emplacement of the Eastern Mourne pluton, N. Ireland: evidence from anisotropy of magnetic susceptibility. J. Geol. Soc. 164, 99–110.
Thiele, R., 1980. Carta Geológica de Chile, Escala 1:250.000, Hoja de Santiago. Carta 39. Instituto de Investigaciones Geológicas, Santiago, Chile, p. 21.
Trubač, J., Žák, J., Chlupáčová, M., Janoušek, V., 2009. Magnetic fabric of the Říčany granite, Bohemian Massif: a record of helical magma flow? J. Volcanol. Geotherm. Res. 181, 25–34.
Vergara, M., Charrier, R., Munizaga, F., Rivano, S., Sepulveda, P., Thiele, R., Drake, R., 1988. Miocene volcanism in the central Chilean Andes (31°30'S-34°35'S). J. South Am. Earth Sci. 1, 199–209.
Vernon, R., 2000. Review of microstructural evidence of magmatic and solid-state flow. Vis. Geosci. 5, 1–23.
Walker Jr., B.A., Miller, C., Lowery Claiborne, L., Wooden, J., Miller, J., 2007. Geology and geochronology of the Spirit Mountain batholith, southern Nevada: implications for timescales and physical processes of batholith construction. J. Volcanol. Geotherm. Res. 167, 239–262.
Žák, J., Kabele, P., 2012. A new approach to modeling perpendicular fabrics in porphyritic plutonic rocks using the finite element method. Int. J. Earth Sci. 101, 715–730.
Žák, J., Paterson, S.R., Memeti, V., 2007. Four magmatic fabrics in the Tuolumne batholith, central Sierra Nevada, California (USA): implications for interpreting fabric patterns in plutons and evolution of magma chambers in the upper crust. Geol. Soc. Am. Bull. 119, 184–201.
Žák, J., Schulmann, K., Hrouda, F., 2005. Multiple magmatic fabrics in the Sázava pluton (Bohemian Massif, Czech Republic): a result of superposition of wrench-dominated regional transpression on final emplacement. J. Struct. Geol. 27, 805–822.
Žák, J., Verner, K., Týcová, P., 2008. Multiple magmatic fabrics in plutons: an overlooked tool for exploring interactions between magmatic processes and regional deformation? Geol. Mag. 145, 537–551.